Applied Cardiopulmonary Pathophysiology 16: 5-16, 2012

# Airway pressure distribution during xenon anesthesia: The insufflation phase at constant flow (volume controlled mode)

*Ira M. Katz[1,2], Andrew R. Martin[1], Chia-Hsiang Feng[1], Caroline Majoral[1], Georges Caillibotte[1], Thomas Marx[1], Jean-Etienne Bazin[3], Christian Daviet[1]*

*[1]Medical Gases Group, Air Liquide Santé International, Centre de Recherche Claude-Delorme, Jouy-en-Josas, France; [2]Department of Mechanical Engineering, Lafayette College, Easton, PA, USA; [3]Service d'Anesthésie-Réanimation, CHU Estaing, Clermont-Ferrand, France*

**Abstract**

There is an increase in pressure necessary to drive xenon insufflation due to increased flow resistance that results from the elevated density and viscosity of xenon-oxygen mixtures. It had been suggested that these higher pressures could be clinically relevant, though results from animal experiments demonstrate otherwise. Numerical simulations in a healthy adult morphology were performed to investigate how these elevated pressures are distributed within the respiratory tract and patient interface as a function of gas concentration, flow rate and endotracheal tube size. The results confirm that there is indeed an increase in pressure needed to drive xenon anesthesia compared to air or oxygen ventilation and that the differences occurred primarily across the endotracheal tube and were found to be much less significant within the lung itself. For all parameters studied, pressure differences between xenon-oxygen and air or oxygen ventilation were found to be negligible in the acinus for the healthy adult male morphology considered, indicating that the increased pressure at the ventilator to drive xenon insufflation is dissipated in the artificial breathing circuit.

**Key words:** xenon, pressure distribution, endotracheal tube, mathematical model

## Introduction

During xenon anesthesia there is known to be an increase in the ventilator pressure necessary to drive xenon-oxygen mixtures compared to ventilating with nitrogen-oxygen mixtures or other anesthetic gases [1]. This increase is attributed to the elevated density and viscosity of xenon-oxygen mixtures that result in increased resistance for laminar or turbulent flow [2-4]. It has been suggested that the higher pressures could be clinically relevant [5]. However, published data from experiments in pigs indicates that the increased pressure is largely dissipated in the airway circuit, in particular the endotracheal tube [1].

The effect of gas properties on respiratory airway resistance has been studied from a fundamental physiological perspective [6-8], in regard to clinical applications [9;10], and based on numerical simulations [11;12]. But there has not been a focused study on the fundamental mechanics of xenon anesthesia

that has presented the pressure distribution throughout the respiratory tract as this type of measurement is not possible in vivo. Our research group has recently presented an analytical model of pressure distribution in the respiratory tract to study effects of low density helium-oxygen mixtures [13]. In this paper we will provide results from the extension of this model to predict the airway pressure distribution throughout the respiratory tract, including the patient interface, during the insufflation phase of xenon anesthesia. Bench-top experiments were performed in order to determine loss coefficients used for calculating the pressure drop across the patient filter and different diameter endotracheal tubes. The calculated results are based on a parametric variation of flow rate, endotracheal tube (ETT) size and xenon concentration. The ultimate goal is to provide a fundamentally sound basis for the further clinical application of xenon anesthesia.

## Methods

### *Analytical model*

The analytical model is described in detail in the previous paper [13]. Briefly, for a constant insufflation flow rate, the pressure at any location in the respiratory tract compared to the alveolar pressure is

$$p - p_{alv} = \rho \sum h - \rho\left(\alpha \frac{V^2}{2}\right) , \qquad (1)$$

where $p$ and $V$ are the pressure and velocity at each location, $\rho$ is the gas density, and $\alpha$ is a coefficient that modifies the kinetic energy term to account for different flow profiles: $\alpha$=1 for a blunt velocity profile and 2 for a parabolic profile. The summation on the right-hand-side of Equation 1 is called the head loss, which represents the sum of all the resistive energy losses per unit mass in the flow path.

In this typical engineering approach, the head losses in all of the straight flow conduits are called "major," and a summation of all the components that change the velocity distribution (acceleration or deceleration of fluid particles), are called "minor." The minor loss occurs in laminar as well as turbulent flow. The summation of head losses is

$$\sum h = \sum_{major} f \frac{L}{D}\frac{V^2}{2} + \sum_{minor} K \frac{V^2}{2} , \qquad (2)$$

where $f$ is called the friction factor for each straight conduit of length $L$ and diameter $D$, and $K$ is a minor loss coefficient for each component (e.g., the bifurcations in the respiratory tract). For laminar fully developed flow $f$ is analytically determined as

$$f = \frac{64}{\mathrm{Re}} , \qquad (3)$$

where Re is the Reynolds number based on $D$ and the density and viscosity of the fluid, $\rho$ and $\eta$, respectively,

$$\mathrm{Re} = \frac{\rho V D}{\eta} . \qquad (4)$$

After substituting Equations 2-4 into Equation 1 it can be shown that the major loss is independent of density for laminar flow. For turbulent pipe flow $f$ has historically been determined empirically. For smooth tubes the correlation derived by Blasius can be used:

$$f = \frac{0.316}{Re^{0.25}} \qquad (5)$$

The criterion used herein for differentiating laminar and turbulent flow was Re≥2000.

The lungs are modeled as a symmetric, dichotomously branching network of stiff cylindrical tubes (the source of major losses) segmented into a series of bifurcating elements (the source of minor losses). The 23 generations (increasing incrementally from 0 at the trachea) are based on a morphology model for healthy adult male lungs; that is, mother and daughter diameters, length, and

branching angle (θ=70°) at each bifurcation are specified. The minor loss coefficients, $K_{Bif}$, were previously calculated based on computation fluid dynamics simulations [13]. In the present work the patient interface is broken into two components, the filter and the ETT and the minor loss coefficients, $K_{filter}$ and $K_{ETT}$, respectively, were determined through the bench top experiments described in the next section. To model expiratory flow in one example, a small minor loss coefficient of 0.36 was used to account for resistance of the expiratory breathing circuit downstream from the ETT and filter. A schematic of the model is shown in Figure 1. Property values at 1 atm and 37 °C for the gases used in the calculations are presented in Table 1 [14].

### Loss Coefficient Experiments

The minor loss coefficients for the patient filter and ETTs were determined by measuring the pressure drop ($\Delta p$) across them under controlled flow conditions using medical air (Air Liquide, $N_2/O_2$ of 78/22%). A schematic of the experimental system (with an ETT in place) is shown in Figure 2. Three ETTs (Rüsch, Germany) with inside diameters (ID) of 6, 7, and 8 mm and lengths of 28, 31.5, and 33 cm, respectively, were tested. In addition, one breathing filter (Hydro-Guard Mini; Intersurgical, UK) was tested. Two pressure sensors were used: one for low range measurements of 0-5 cm $H_2O$ (PX-277; Omega, US) coupled to a computer based data acquisition system based on LabVIEW software (National Instruments, USA); and the other for high range measurements of 5-100 cm $H_2O$ (PR-201; Eurolec, Ireland). The flow rate

*Table 1: Property values at 1 atm. and 37°C.*

| Gas | Viscosity x10$^5$ (kg/s-m) | Density (kg/m$^3$) |
|---|---|---|
| Medical Air ($N_2/O_2$ 78/22%) | 1.809 | 1.201 |
| Oxygen ($O_2$ 100%) | 2.113 | 1.257 |
| Xenon ($Xe/O_2$ 50/50%) | 2.386 | 3.394 |
| Xenon ($Xe/O_2$ 60/40%) | 2.395 | 3.599 |
| Xenon ($Xe/O_2$ 70/30%) | 2.397 | 3.989 |

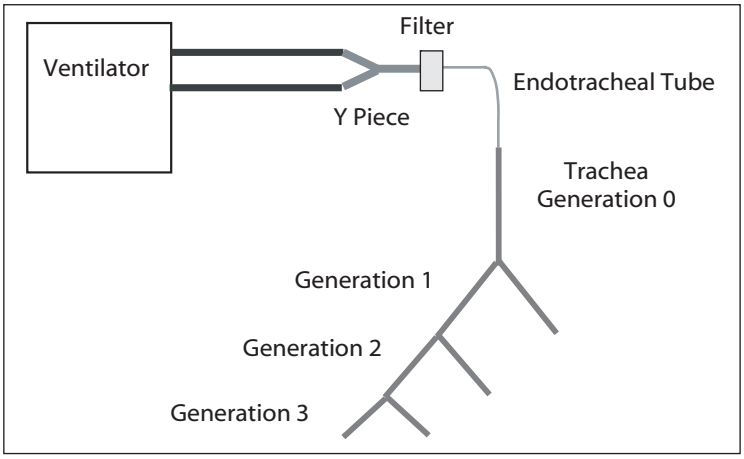


*Figure 1: Schematic basis for the analytical model of pressure loss.*

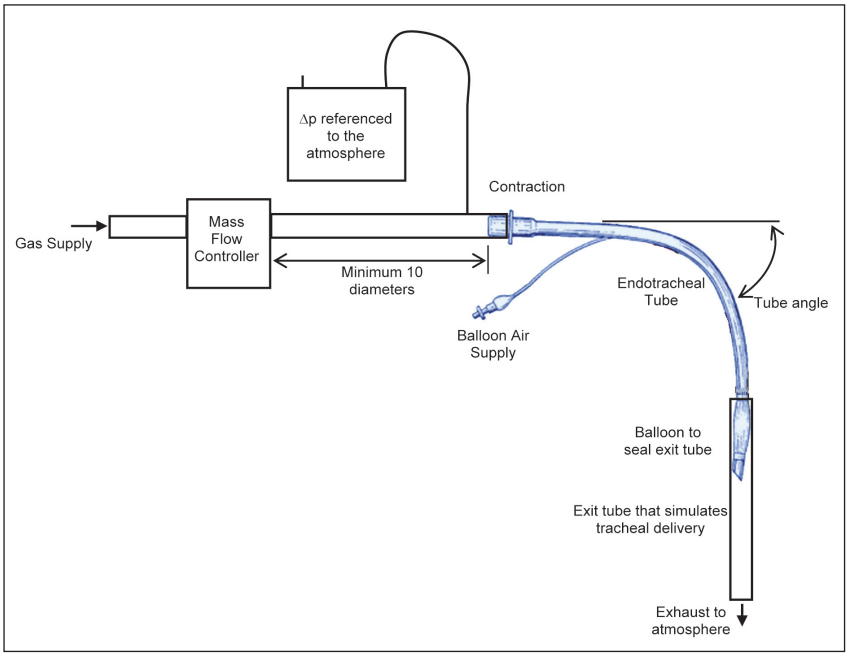


*Figure 2: Schematic of the experimental system used for measuring the loss coefficients for the endotracheal tubes.*

was controlled with a mass flow controller (EL-Flow; Bronkhorst, Netherlands). The inlet and out tubing were 18 mm ID ventilator tubing. Data were taken for flows of 5-100 L/min, at 5 L/min increments. The minor loss coefficient at each flow rate was then calculated based on the pressure drop between the inlet to the tube (or filter) and the atmosphere:

$$K = \frac{2\Delta p}{\rho V^2}.$$

These data were then fit as a function of Re for use in the model. As noted above, all of the experiments were conducted with medical air at room temperature; because the results are correlated with respect to the non dimensional parameter, Re, they can be applied to xenon using the principles of dynamic similitude. As an example, Table 2 lists the Re for the 7 mm ETT and equivalent flow rates for xenon at 37 °C.

## Results

Parametric numerical simulations spanning typical clinical conditions were performed by varying ETT size (6, 7, and 8 mm), flow rate (10, 20, and 30 L/min) and xenon concentration in the anesthetic range (50, 60, and 70% by volume). The pressure distribution versus position in the respiratory tract for the intermediate case of 7 mm, 20 L/min, and 60% xenon is shown in Figure 3 compared with equivalent curves for medical air and 100% oxygen. This distribution represents the difference in pressure between a position of interest and the deepest generation of alveoli. The first point in the curve is this pressure difference at the Y-piece; the second is the pressure difference from after the filter; and the third is the pressure difference from immediately after the ETT in the trachea. The patient filter is included following the practice in Europe. For applications without filters the associated effect on the pressure distribution can be disregarded. The remaining numbered positions represent the bronchial gen-

*Table 2: Experimental flow rates with medical air, the Re calculated for the 7 mm endotracheal tube with property values at 20°C ($\eta$=1.809x10$^{-5}$ kg/s-m, $\rho$=1.207 kg/m$^3$), and the equivalent flow rates of xenon at 37°C.*

| Experimental Flow Rate with Medical Air (L/min) | Re (D=7 mm) | Equivalent Flow Rate with Xenon (L/min) |
|---|---|---|
| 5 | 1006 | 2.2 |
| 10 | 2013 | 4.4 |
| 15 | 3019 | 6.6 |
| 20 | 4025 | 8.8 |
| 25 | 5032 | 11.0 |
| 30 | 6038 | 13.3 |
| 35 | 7044 | 15.5 |
| 40 | 8051 | 17.7 |
| 45 | 9057 | 19.9 |
| 50 | 10063 | 22.1 |
| 55 | 11070 | 24.3 |
| 60 | 12076 | 26.5 |
| 65 | 13082 | 28.7 |
| 70 | 14089 | 30.9 |
| 75 | 15095 | 33.1 |
| 80 | 16101 | 35.3 |
| 85 | 17108 | 37.6 |
| 90 | 18114 | 39.8 |
| 95 | 19120 | 42.0 |
| 100 | 20127 | 44.2 |

erations. Thus, position 0 is at a point just beyond the first bifurcation (i.e. entering generation 1). Figures 4, 5, and 6 show the pressure distributions for the parametric variation of ETT size, flow rate, and xenon concentration, respectively.

In Figure 3A, for the intermediate case, it can be seen that the pressure at the Y-piece to drive xenon insufflation is almost two times (97% more than) that necessary for 100% oxygen.

At the exit to the ETT, the pressure is still 78% greater with xenon than with 100% oxygen, but the values themselves are approximately one tenth of what they were at the Y-piece. In other words, 90% of the pressure drop occurs in the external breathing circuit (i.e., the filter and ETT). Within the lung (as shown in Figure 3B) P - $P_{alv}$ dissipates to essentially zero after generation 15, which marks the entry to the acinus, for all the gas mixtures considered.

Parametric variation of ETT size, flow rate and xenon concentration were performed. In Figure 4 it can be seen that the ETT size has a significant effect on the pressure at the Y-piece: there is a 130% increase for a 6mm tube compared to an 8mm tube for 60% xenon flowing at 20 L/min. However, note that in the lung itself the pressure distributions are identical. Figure 5 shows the effect of flow rate for 60% xenon through a 7 mm ETT. At the Y-piece, there is an increase in pressure of more than 450% increasing the

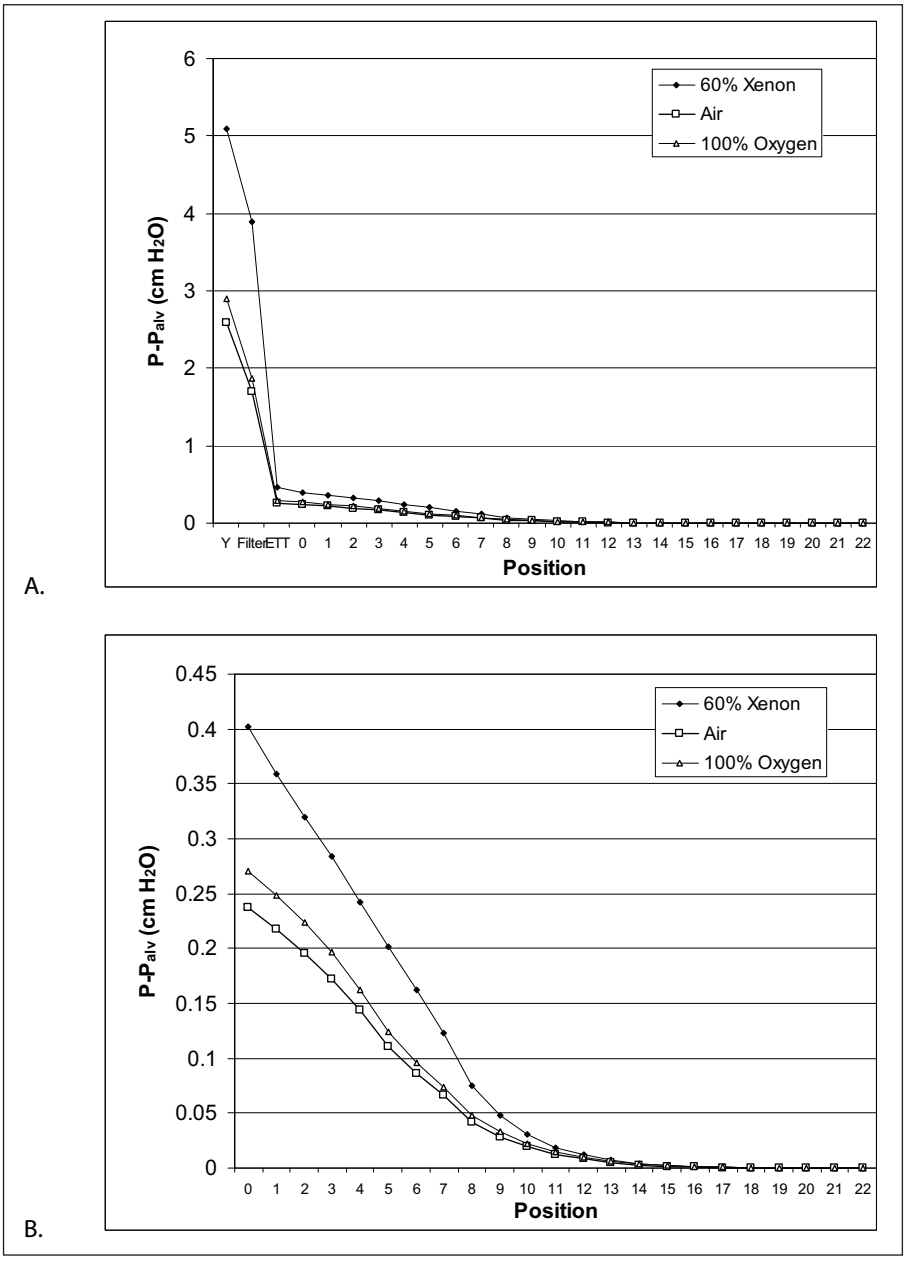


*Figure 3: Pressure distribution in the respiratory tract for the standard case of 7 mm, 20 L/min, and 60% xenon compared to medical air and 100% oxygen: A) complete distribution, B) only within the lung.*

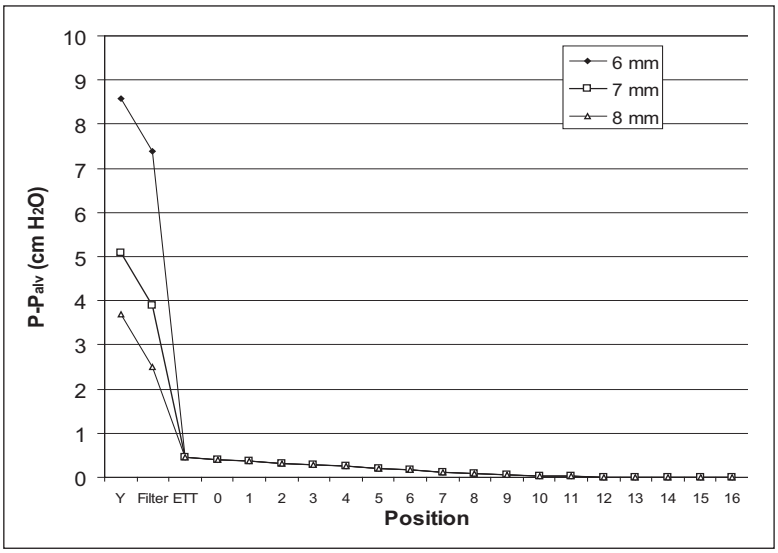


*Figure 4: Pressure distributions in the respiratory tract based on the variation of EET size for 60% xenon concentration and 20 L/min flow rate.*

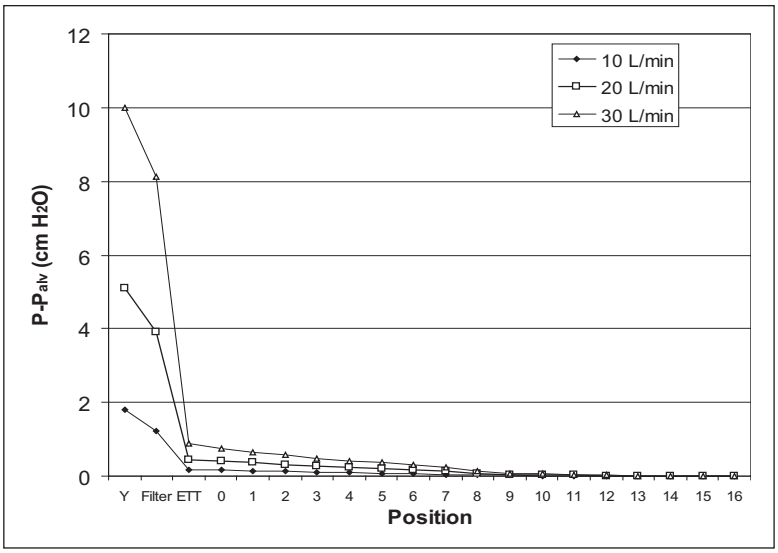


*Figure 5: Pressure distributions in the respiratory tract based on the variation of flow rate for a 7 mm endotracheal tube and 60% xenon concentration.*

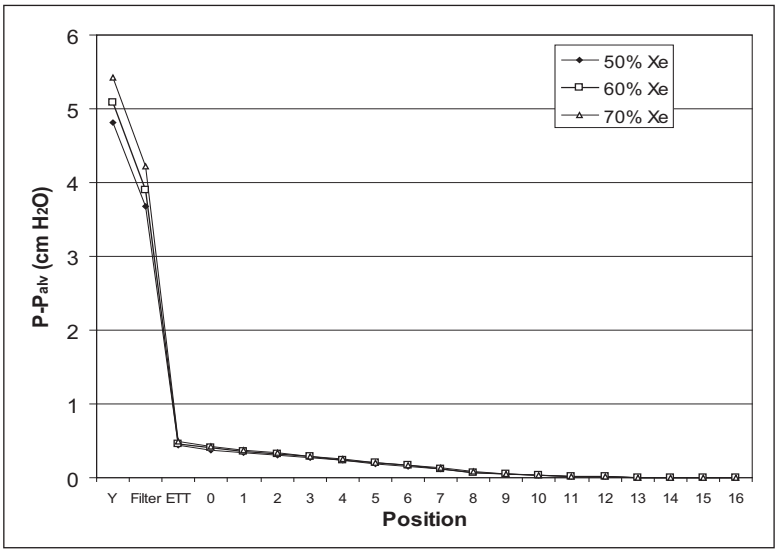


*Figure 6: Pressure distributions in the respiratory tract based on the variation of xenon concentration for 20 L/min flow rate and a 7 mm endotracheal tube.*

flow rate from 10 to 30 L/min. There are relatively equivalent increases in pressure within the lung. Finally, as shown in Figure 6, variation of the xenon concentration from 50% to 70% has relatively little effect on the pressure distribution (increasing pressure by about 12% at the Y-piece).

## Discussion

Pressure distribution representing the difference in pressure between positions of interest in the respiratory tract, including the external breathing circuit, with respect to the deepest generation of alveoli have been presented in Figures 3-6. Because the relative alveolar pressures are essentially zero for all the cases considered, the results are consistent with the conclusion of Schmidt et al. [1] that there is little risk of impairment of the bronchial system due to the elevated pressures needed to drive xenon anesthesia under normal conditions.

The pressure distributions shown in Figures 3-6 are most directly applicable for constant flow insufflation. However, they can also be seen as the instantaneous pressure distributions that would exist in any ventilation mode. These pressure distributions are not available in practice but only the Y-piece pressure as measured by the anesthesia ventilator. To put the results into perspective the following example is introduced: constant insufflation flow rate (40 L/min) in volume controlled mode with ventilation parameters of 0.5 L tidal volume at 20 breaths/minute and an inspiratory:expiratory ratio of 1:3, through a 7 mm endotracheal tube with a one second pause to create a plateau, into a lung with compliance of 0.03 L/cm $H_2O$. Figure 7 shows time traces over the breathing cycle for the A) flow rate and B) pressure at the Y-piece as would be seen at the ventilator for 100% oxygen and for 60-40% xenon-oxygen.

A description of the breathing cycle will define the terms introduced in Figure 7. The breath itself begins at t=0 with an idealized instantaneous increase in insufflation flow rate from 0 to 40 L/min as shown in Figure 7.A. The change in pressure needed to overcome the flow resistance ($\Delta p_{res}$) for each gas is indicated in Figure 7.B. As discussed previously, this pressure is dependant on the gas properties, especially density, and is therefore greater for the xenon mixture than for oxygen. The constant insufflation continues for 0.75 s until the target tidal volume of 0.5 L is achieved. The pressure needed to drive this flow must increase to the peak pressure

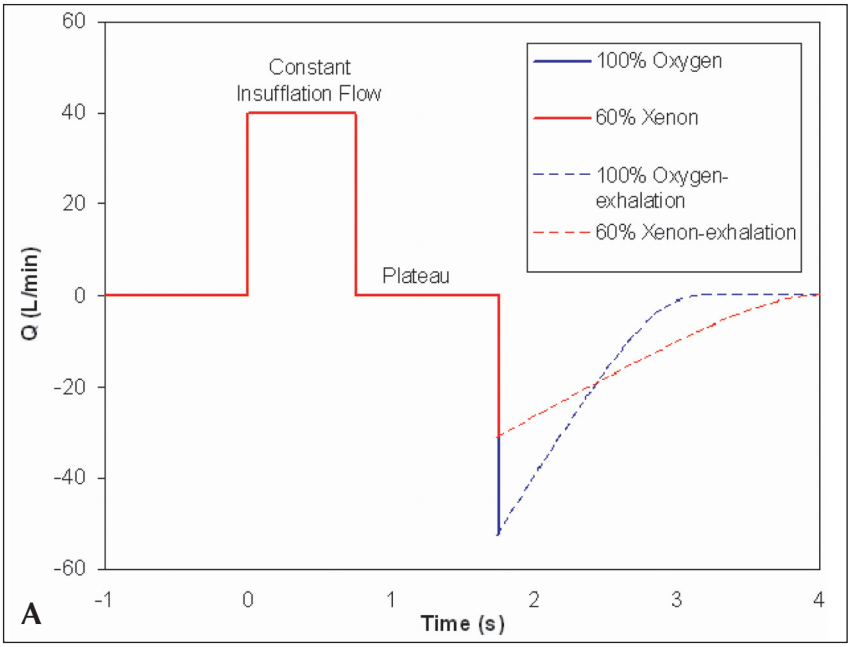
60
40
20
0
-20
-40
-60
Q (L/min)
Constant
Insufflation Flow
Plateau
100% Oxygen
60% Xenon
100% Oxygen-
exhalation
60% Xenon-exhalation
-1
0
1
2
3
4
Time (s)
A

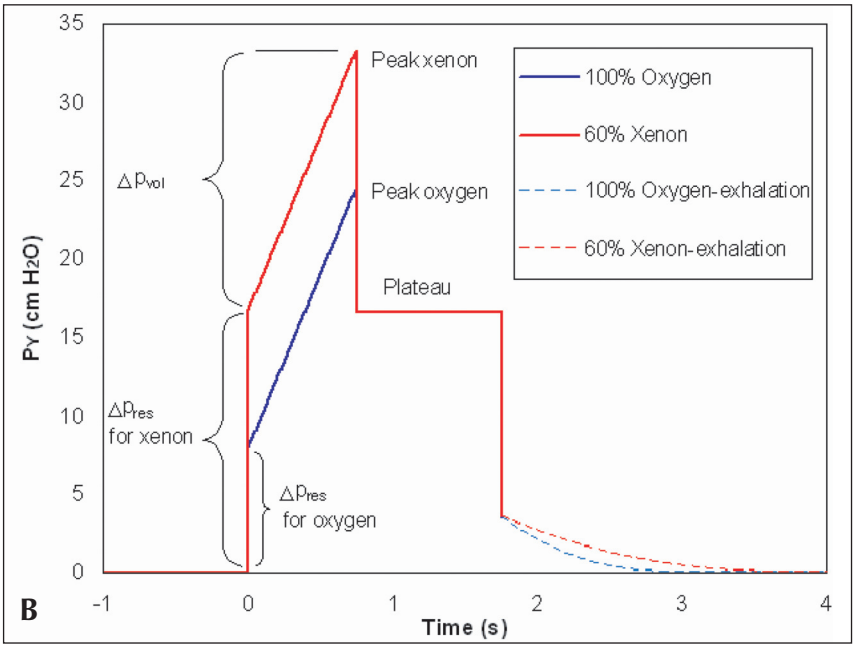
35
30
25
20
15
10
5
0
PY (cm H2O)
Peak xenon
Peak oxygen
Plateau
ΔPvol
ΔPres
for xenon
ΔPres
for oxygen
100% Oxygen
60% Xenon
100% Oxygen-exhalation
60% Xenon-exhalation
-1
0
1
2
3
4
Time (s)
B

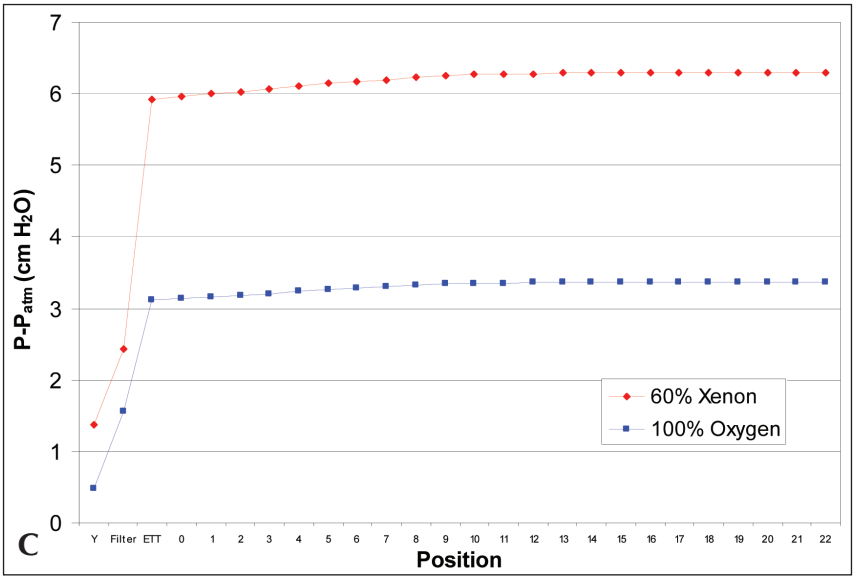


*Figure 7: Model predictions with ventilation parameters of 0.5 L tidal volume at 20 breaths/minute and an inspiratory:expiratory ratio of 1:3 (constant insufflation, 40 L/min), through a 7 mm endotracheal tube with a one second pause to create a plateau, into a lung with compliance of 0.03 L/cm $H_2O$: A) flow rate and B) pressure as measured at the Y-piece. The exhalation curves are dashed to indicate that they represent estimates for a hypothetical flow circuit. C) Pressure distributions in the respiratory tract at 2.45 s where the exhalation flow rates are the same (19.33 L/min).*

($\Delta p_{vol}$) because the alveolar pressure is increasing according to the lung compliance. Because the flow rate, tidal volume and compliance are the same for both gases, the slope of the pressure rise and $\Delta p_{vol}$ are the same for both gases. In particular, for this example $\Delta p_{vol}$= 0.5 L / 0.03 L/cm $H_2O$ = 16.7 cm $H_2O$. The peak pressures are different due to the difference in $\Delta p_{res}$ between the xenon mixture and oxygen. But recall from the previous discussion of Figure 3, the alveolar pressure in each case will be essentially the same. When the target tidal volume has been achieved the flow is stopped and because the volume is held in the lung there is a plateau pressure for 1 s from 0.75 to 1.75 s. With no flow the pressure measured at the Y-piece, the plateau pressure, is the same as the airway pressure and is the same for both gases and is equal to $\Delta p_{vol}$. At this point the ventilator releases the pressure to allow exhalation. The exhalation curves are shown as dashed lines because they represent a hypothetical case where specific curves would be dependent on the flow resistance in the exhalation circuit of the ventilator. However, it is certain that the xenon mixture will have a longer exhalation time constant than oxygen due to its higher flow resistance. Anecdotally, some physicians have reported higher plateau pressures during xenon anesthesia, which could be a result of end-expiratory gas trapping. The plateau pressure is elevated for over-inflated lungs because lung compliance decreases as lung volume increases towards total lung capacity.

Examining Figure 7B in more detail we note that the peak pressure at the Y-piece for the xenon mixture is over 33 cm $H_2O$ which is about two times greater than for oxygen. However, the pressure at the Y-piece is the same as airway pressure only when there is no flow. Thus the plateau pressure is often approximated as airway pressure [15], which is about 16 cm $H_2O$ in this case.

Figure 7C shows the pressure distributions for each gas at 2.45 s, when the exhalation flow rates are the same (19.33 L/min). The higher pressures throughout the lung during xenon exhalation (about 6 versus 3 cm $H_2O$ in this example) result from slower lung emptying due primarily to the greater resistance of the ETT.

It should be noted that this is a focused study that does not address other issues related to the mechanics of xenon anesthesia such as the effects of disease (e.g. central vs. peripheral airway obstruction), and the morphology of sub-populations (e.g. infants, children). Furthermore, herein is only a limited treatment of exhalation. The links between these mechanical effects and gas exchange also merit further study.

Regarding the specific methods used, it has been reported in the literature that for turbulent flow pressure losses in ETTs can be modeled with the Blasius equation (Equation 5) [16;17]. Herein the ETT is consider a minor loss, so we might expect $K_{ETT}=fL/D$ for the ETT, with f determined using Equation 5. However, in our experiments the measured values were greater than the Blasius result. This discrepancy can be accounted for by the additional losses due to the contraction into the ETT and the expansion into the trachea (see Figure 2). As these losses would be part of the breathing circuit they are included implicitly within $K_{ETT}$ in the model. On the other hand, pressure drop through the larger connecting ventilator tubing is assumed to be negligible. It has also been noted in the literature that effects due to curvature in ETTs are minimal for turbulent flow [17]. We found this to be true in our experiments. For example, for the 7 mm tube at Re=10000 (Q=50 L/min in air, about 22 L/min for 60% xenon) the difference in *K* value between a straight tube and a 90° bend was about 6%. As the bend angle is not fixed in practice, we based the calculations on $K_{ETT}$ for straight tubes.

In conclusion, numerical simulations of the insufflation phase at constant flow (Volume Controlled mode) for xenon anesthesia have been performed for a healthy adult male morphological model, showing that a higher peak pressure is needed at the Y-piece than for air or oxygen to achieve the same ventilation pattern. However, the pressure differences were much less significant within the lung itself, and negligible in the acinus. The pressure at the Y-piece during insufflation is to a great extent dependent on the flow rate and the size of the ETT used; but to a much lesser extent on the concentration of xenon in the mixture when this falls within the anesthetic range. As has been demonstrated in animals [1], this work confirms in a numerical model of human airways that the increased pressure at the ventilator to drive xenon insufflation is dissipated in the artificial breathing circuit over a range of ventilatory conditions.

## References


1. Schmidt M, Marx T, Papp-Jambor C, Reinelt H, Schirmer U. Airway pressures during xenon anaesthesia. Appl Cardiac Pathophysiol 2009; 13: 208-11
2. Baumert J-H, Reyle-Hahn M, Hecker K, Tenbrinck R, Kuhlen R, Rossaint R. Increased airway resistance during xenon anaesthesia in pigs is attributed to physical properties of the gas. Brit J Anaesth 2002; 88: 540-5
3. Zhang P, Ohara A, Mashimo T, Imanaka H, Uchiyama A, Yoshiya I. Pulmonary resistance in dogs: a comparison of xenon with nitrous oxide. Can J Anaesth 1995; 547-53
4. Dingley J, Ivanova-Stoilova TM, Grundler S, Wall T. Xenon: recent developments. Anaesthesia 1999; 54: 335-46
5. Rueckoldt H, Vangerow B, Marx G, Haubitz B, Cobas Meyer M, Piepenbrock S, Leuwer M. Xenon inhalation increases airway pressure in ventilated patients. Acta Anaest Scan 1999; 43: 1060-4
6. DeWeese EL, Sullivan TY, Yu PL. Ventilatory and occlusion pressure responses to helium breathing. J Appl Physiol 1983; 54: 1525-31
7. Staats BA, Wilson TA, Lai-Fook SJ, Rodarte JR, Hyatt RE. Viscosity and density dependence during maximal flow in man. J Appl Physiol 1980; 48: 313-9

8. Wood LDH, Bryan AC. Effect of increased ambient pressure on flow-volume curve of the lung. J Appl Physiol 1969; 27: 4-8
9. Despas PJ, Leroux M, Macklem PT. Site of airway obstruction in asthma as determined by measuring maximal expiratory flow breathing air and a helium-oxygen mixture. J Clin Inv 1972; 51: 3235-43
10. Jaber S, Fodil R, Carlucci A, Boussarsar M, Pigeot J, Lemaire F, Harf A, Lofaso F, Isabey D, Brochard L. Noninvasive ventilation with helium-oxygen in acute exacerbations of chronic obstructive pulmonary disease. AJRCCM 2000; 161: 1191-200
11. Brighenti C, Barbini P, Gnudi G, Cevenini G, Pecchiari M, Angelo ED. Helium-oxygen ventilation in the presence of expiratory flow-limitation: A model study. Respir Physiol Neurobiol 2007; 157: 326-34
12. Papamoschou D. Theoretical validation of the respiratory benefits of helium-oxygen mixtures. Respir Physiol 1995; 99: 183-90
13. Katz IM, Martin AR, Muller P-A, Terzibachi K, Feng C-H, Caillibotte G, Sandeau J, Texereau J. The Ventilation Distribution of Helium-Oxygen Mixtures and the Role of Inertial Losses in the Presence of Heterogeneous Airway Obstructions. J Biomech 2011; 44: 1137-43
14. Katz IM, Caillibotte G, Martin AR, Arpentinier P. Property Value Estimation for Inhaled Therapeutic Binary Gas Mixtures: He, Xe, $N_2O$, and $N_2$ with $O_2$. Med Gas Res 2011; in press.
15. Gattinoni L, Protti A, Caironi P, Carlesso E. Ventilator-induced lung injury: The anatomical anti physiological Framework. Crit Care Med 2010; 38: S539-S548
16. Jarreau P-H, Louis B, Dassieu G, Desfrere L, Blanchard PW, Moriette G, Isabey D, Harf A. Estimation of inspiratory pressure drop in neonatal and pediatric endotracheal tubes. J Appl Physiol 1999; 87: 36-46
17. Lichtwarck-Aschoff M, Helmer A, Kawati R, Lattuada M, Sjöstrand UH, Zügel N, Guttman J, Hedenstierna G. Good short-term agreement between measured and calculated tracheal pressure. Brit J Anaesth 2003; 91: 239-48

*Correspondence address*
Ira Katz
Medical Gases Group
Centre de Recherche Claude-Delorme
1 chemin de la Porte des Loges
Les Loges-en-Josas, B.P. 126
78354 Jouy-en-Josas Cedex
France
ira.katz@airliquide.com